Carbon geochemistry of plankton-dominated samples in the Laptev and East Siberian shelves: contrasts in suspended particle composition

Tesi Tommaso [1,2,3], Marc C. Geibel [1,2], Christof Pearce [2,4,5], Elena Panova [6], Jorien E. Vonk [7], Emma Karlsson[1,2], Joan A. Salvado[1,2], Martin Kruså[1,2], Lisa Bröder [1,2], Christoph Humborg [1,2], Igor Semiletov[6,8,9], Örjan Gustafsson [1,2]

[1] Department of Environmental Science and Analytical Chemistry (ACES), Stockholm University

[2] Bolin Centre for Climate Research, Stockholm University

[3] Institute of Marine Sciences, National Research Council (ISMAR-CNR)

[4] Department of Geological Sciences, Stockholm University, Sweden

[5] Department of Geoscience, Aarhus University, Denmark

[6] Tomsk Polytechnic University

[7] Vrije Universiteit Amsterdam (VU)

[8] Pacific Oceanological Institute FEB RAS

[9] University of Alaska Fairbanks

Abstract

Recent Arctic studies suggest that sea-ice decline and permafrost thawing will affect phytoplankton dynamics and stimulate heterotrophic communities. However, in what way the plankton composition will change as the warming proceeds remains elusive. Here we investigate the chemical signature of the plankton-dominated fraction of particulate organic matter (POM, >10μm) collected along the Siberian shelf. POM (>10μm) samples were analysed using molecular biomarkers (CuO oxidation and IP$_{25}$) and dual-carbon isotopes (δ^{13}C and Δ^{14}C). In addition, surface water chemical properties were integrated with the POM (>10μm) dataset to understand the link between plankton composition and environmental conditions.

δ^{13}C and Δ^{14}C exhibited a large variability in the POM (>10μm) distribution while terrestrial biomarkers showed a negligible input from terrestrial sources. In the Laptev Sea (LS) open-waters, δ^{13}C and Δ^{14}C fingerprint of POM (>10μm) suggested that dissolved organic carbon (DOC) from the Lena river was the primary source of metabolisable carbon indicating, thus, a heterotrophic environment. Moving eastwards toward the sea-ice dominated East Siberian Sea (ESS), the system became progressively more autotrophic. Comparison between δ^{13}C of POM (>10μm) samples and CO$_2$aq concentrations revealed that the carbon isotope fractionation increased moving toward the easternmost and most productive stations.

In a warming scenario characterized by enhanced terrestrial DOC release (thawing permafrost) and progressive sea-ice decline, heterotrophic conditions might persist in the LS while the nutrient-rich Pacific inflow will likely stimulate greater ~~ESS~~ primary productivity in the ESS. The contrasting trophic conditions will result in a sharp gradient in δ^{13}C between the LS and ESS similar to what documented in our semi-synoptic study.

1. Introduction

The progressive reduction of sea-ice extent in the Arctic Ocean is indisputable evidence of modern global warming (Comiso et al., 2008; Ding et al., 2017; Kwok and Rothrock, 2009). The unprecedented decline of sea-ice is expected to alter several aspects of the Arctic marine ecology such as plankton abundance and its temporal distribution (Arrigo et al., 2008). For instance, recent studies suggest that the increase of solar irradiance will stimulate greater primary productivity in summer while the prolonged ice-free conditions will develop a second algal bloom in early fall, which is a distinctive feature of only lower latitudes (Ardyna et al., 2014; Lalande et al., 2009; Lalande et al., 2014). The phytoplankton communities are expected to profoundly change towards a higher contribution from open water phytoplankton at the expense of sea-ice assemblages (Fujiwara et al., 2014). Taken together, a greater productivity in the ice-free or marginal ice zone compare to the multi-year ice system, is also expected to lead to greater carbon uptake and settling export of organic carbon from the surface to deeper strata of the Arctic Ocean (Gustafsson and Andersson, 2012).

Sea-ice decline will also affect the water-air gas exchange, currents and river plume dispersion which, in turn, exert large control on the surface water chemical/physical properties (Aagaard and Carmack, 1989; Ardyna et al., 2014; Lalande et al., 2014). On top of this, destabilization of permafrost soils and the terrestrial cryosphere will result in enhanced particulate and dissolved carbon input to the Arctic Ocean (Frey and Smith, 2005; Vonk et al., 2012). As a result, the geochemical signature of both autotrophic and heterotrophic plankton communities is also expected to change as the warming proceeds. However, how the warming will ultimately affect the marine geochemical signal is poorly understood. This study seeks a better understanding of the chemical composition of plankton that dominates regions of the Arctic Ocean characterized by different sea-ice coverages, nutrient availability and riverine

76   influence. In particular, we focus on the carbon isotope fingerprint (i.e. $\delta^{13}C$ and $\Delta^{14}C$) of

77   plankton that grows in ice-covered and ice-free Marginal Ice Zone (MIZ) regimes on the

78   Siberian margin. The motivation behind investigating the chemical fingerprint of plankton

79   from different regimes is to provide a better understanding of the carbon signature for direct

80   applications to carbon studies of both modern systems and paleo-reconstructions. In

81   particular, the isotope composition of marine OC finds several applications in climate,

82   ecology and carbon source apportionment studies. For example, stable carbon isotopes of

83   marine phytoplankton are used for paleo-pCO_2 reconstructions over geological time scales

84   (Hoins et al., 2015; Pagani et al., 1999; Popp et al., 1999; Rau, 1994). The $\delta^{13}C$ signature also

85   provides a solid tool for marine food web and ecosystem structure investigations (Dunton et

86   al., 2006; Iken et al., 2005; Kohlbach et al., 2016). Furthermore, dual-carbon isotope mixing

87   models ($\delta^{13}C$ and $\Delta^{14}C$) are commonly used to quantify the relative proportion of marine and

88   various allochtonous sources (e.g., permafrost soil) in both contemporary and paleo-

89   reconstructed carbon cycling of the Arctic (Karlsson et al., 2016; Tesi et al., 2016; Vonk et

90   al., 2012; Vonk et al., 2014).

91   With this overarching goal in mind, here we investigate the >10 μm fraction of

92   particulate organic matter (POM) in ice-covered and ice-free MIZ regimes of the Siberian

93   Arctic Shelf during the SWERUS-C3 expedition (July-August 2014) (Fig. 1). The plankton-

94   dominated POM samples collected throughout the ca. 4,500 km long cruise track were

95   characterized using bulk parameters (OC, $\delta^{13}C$ and $\Delta^{14}C$) and biomarkers (highly branched

96   isoprenoids, IP_{25}; CuO oxidation products). In addition, continuous measurements of

97   dissolved CO_2 (CO_{2aq}) and its stable carbon isotope composition ($\delta^{13}C_{CO2}$) were performed

98   during the campaign (Humborg et al., 2017) and used for a direct comparison with the

99   chemical composition of the POM fraction.

100

4

2. Study region

The Laptev Sea and the East Siberian Sea are shallow epicontinental seas in the Russian Arctic separated by the New Siberian Islands (Fig. 1). Sea-ice cover lasts for most part of the year over the shelf. Late spring/summer is characterized by the seasonal sea-ice retreat coupled with river freshet which supplies large amount of terrestrial carbon in the form of particulate and dissolved matters (Karlsson et al., 2016; Salvadó et al., 2016; Sánchez-García et al., 2011). The Lena (523 km3/y), Indigirka (54 km3/y), and Kolyma (48 km3/y) are the major rivers (Gordeev, 2006). During the ice-free season, the Lena plume can be traced in the outer-shelf of the Laptev Sea (Fichot et al., 2013; Salvadó et al., 2016; Sánchez-García et al., 2011) while Pacific inflow from the Bering strait affects further east the East Siberia margin (Semiletov et al., 2005). The Pacific inflow exerts control on the nutrient balance as it supplies nitrates and nitrites to an otherwise nutrient-depleted region (Anderson et al., 2011; Semiletov et al., 2005). Another important source of particulate material to the continental margin is the Pleistocene Ice Complex Deposit (ICD) entering the ocean via coastal erosion (Lantuit et al., 2011; Vonk et al., 2012) which is the dominant carbon source between the Kolyma river and the Lena river (Vonk et al., 2012).

3. Methods

3.1 POM (<10 μm) sampling

Seawater was pumped from a stainless steel inlet on the hull of the icebreaker *Oden* positioned at 8 m below the sea surface. The inlet system is tested and further described in Sobek and Gustafsson (2004) and Gustafsson et al. (2005). Figure 1a and 1b show the regions covered to harvest each POM (>10 μm) sample with their location shown as time-averaged position. The particulate material was retained via a large volume filtration apparatus using a 10-μm Nitex® (nylon) mesh placed in a 29.3 cm filter holder. After collection, filtered

126 particulate material was transferred in pre-clean HDPE tubes by rinsing the Nitex® filters

127 with MilliQ water. Samples were kept frozen throughout the expedition. In the lab, samples

128 were transferred in pre-cleaned Falcon® tubes (rinsed with 0.1M HCl) and gently centrifuged

129 to remove the supernatant. The residual particulate material was frozen and subsequently

130 freeze-dried prior to biogeochemical analyses.

131

132 3.2 Bulk carbon isotopes and biomarker analyses

133 Organic carbon (OC) and stable carbon isotope ($\delta^{13}C$) analyses were carried out on

134 acidified samples (Ag capsules, HCl, 1.5M) to remove the carbonate fraction (Nieuwenhuize

135 et al., 1994). Analyses were performed using a Thermo Electron mass spectrometer directly

136 coupled to a Carlo Erba NC2500 Elemental Analyzer via a Conflo III (Department of

137 Geological Sciences, Stockholm University). OC values are reported as weight percent

138 (%d.w.) whereas stable isotope data are reported in the conventional $\delta^{13}C$ notation (‰). The

139 analytical error for $\delta^{13}C$ was lower than ±0.1‰ based on replicates. Acidified (HCl, 1.5 M)

140 samples for radiocarbon abundance were analysed at the US-NSF National Ocean Science

141 Accelerator Mass Spectrometry (NOSAMS) facility (Woods Hole Oceanographic Institution,

142 Woods Hole, USA). Radiocarbon data are reported in the standard $\Delta^{14}C$ notation (‰).

143 Alkaline CuO oxidations were carried out using an UltraWAVE Milestone microwave

144 as described in Tesi et al. (2014). Briefly, about 2 mg of OC was oxidised using CuO under

145 alkaline (2N NaOH) and oxygen-free conditions at 150 °C for 90 min in teflon tubes. After

146 the oxidation, known amounts of recovery standards (trans-cinnamic acid and ethylvanillin)

147 were added to the solution. The NaOH solutions were then acidified to pH 1 with

148 concentrated HCl and extracted with ethyl acetate. Extracts were dried and redissolved in

149 pyridine. CuO oxidation products were quantified by GC-MS in full scan mode (50-650 m/z).

150 Before GC analyses, the CuO oxidation products were derivatized with bis(trimethylsilyl)

151   trifluoroacetamide+1% trimethylchlorosilane at 60°C for 30 min. The compounds were

152   separated chromatographically in a 30m×250 μm DB5ms (0.25 μm thick film) capillary GC

153   column, using an initial temperature of 100°C, a temperature ramp of 4°C/min and a final

154   temperature of 300°C. Lignin phenols (terrestrial biomarkers) were quantified using the

155   response factors of commercially available standards (Sigma-Aldrich) whereas the rest of the

156   CuO oxidation products were quantified by comparing the response factor of trans-cinnamic

157   acid. Lignin-derived reaction products include vanillyl phenols (V=vanillin, acetovanillone,

158   vanillic acid), syringyl phenols (S=syringealdehyde, acetosyringone, syringic acid) and

159   cinnamyl phenols (C=p-coumaric acid, ferulic acid). In addition to lignin, cutin-derived

160   products (hydroxyl fatty acids) were used to trace the land-derived input (Goñi and Hedges,

161   1990; Tesi et al., 2010). Other CuO oxidation products include para-hydroxybenzene

162   monomers (P-series), benzoic acids (B-series) and short-chain fatty acids (FA-series) which

163   can have both terrestrial and marine origin (Goñi and Hedges, 1995; Tesi et al., 2010).

164   The sea-ice proxy IP_{25} (mono-unsaturated highly branched isoprenoid (HBI) alkene)

165   was quantified according to Belt et al. (2012). IP_{25} producers are a minor (<5%) fraction of

166   the total sea-ice taxa which are, however, ubiquitous in pan-Arctic sea-ice. Species include

167   *Pleurosigma stuxbergii var. rhomboide*, *Haslea crucigeroides* (and/or *Haslea spicula*) and

168   *Haslea kjellmanii* (Brown et al., 2014a). Briefly, lipids were extracted via sonication using a

169   dichloromethane/methanol solution (2:1 v/v × 3). Prior to the extraction, two internal

170   standards (7-hexylnonadecane, 7-HND and 9- octylheptadecene, 9-OHD) were added to

171   permit quantification of IP_{25} (monounsaturated highly branched isoprenoid) following

172   analysis via GC-MS. Total lipid extracts (TLEs) were dried under N_2 after removing the water

173   excess with anhydrous $NaSO_4$. Dry TLEs were redissolved in dichloromethane and the non-

174   polar hydrocarbon fraction was purified using open column chromatography (deactivated

175 SiO$_2$) and hexane as eluent. Saturated and unsaturated n-alkanes were further separated using

176 10% AgNO$_3$ coated silica gel using hexane and dichloromethane, respectively.

177   Quantification of IP$_{25}$ was carried out in SIM mode (*m/z* 350.3) as described in Belt et

178 al. (2012). The GC was fitted with a 30m×250 µm DB5ms (0.25 µm thick film) capillary GC

179 column. Initial GC oven temperature was set to 60°C followed by a 10°C/min ramp until a

180 final temperature of 310°C (hold time 10 min).

181

182 **3.3. Microscope images of plankton**

183   High resolution digital images were taken with an Environmental Scanning Electron

184 Microscope (ESEM) Philips XL30 FEG in high voltage (15kV) and magnification 250X.

185 Samples were further studied for identification of diatoms and dinoflagellates using a

186 transmitted light microscope (Leitz Laborlux 12 Pol) equipped with differential interference

187 contrast optics at 1000X magnification. Microscope slides were prepared using settling

188 chambers to achieve an even distribution of particles on the cover glass, regardless of size and

189 shape Warnock and Sherer (2014).

190 **3.4 Sea-ice data**

191   Daily AMSR2 sea-ice extent and concentration maps were provided by the Institute of

192 Environmental Physics, University of Bremen, Germany (Spreen et al., 2008) as GeoTIFF

193 files (ftp://seaice.uni-bremen.de).

194

195   **3.5 Statistics** We used two-tailed T-test (homoscedasticity) and Welch T-test

196 (heteroskedasticity) to assess whether the differences between open waters and sea-ice

197 dominated waters were statistically significant. For this study, significance level (alpha) was

198 set at 0.01.

199

4. Surface water conditions during the SWERUS-C3 expedition

Before discussing the chemical composition of the POM (>10 μm), here we briefly introduce the different environmental conditions encountered throughout the cruise track. The surface water data presented in this section were pulled together from previous studies which provide an in-depth analysis of the surface water properties during the SWERUS-C3 expedition in 2014 (Humborg et al., 2017; Salvadó et al., 2016) (Table 2). For this study, continuous CO_2aq and $\delta^{13}C_{CO2}$ data (Humborg et al., 2017) were averaged to match the water sampling stations allowing for a direct comparison with DOC and salinity data (Fig.2) (Supplementary Material).

Summer 2014 was consistent with the long-term downward trend in Arctic sea-ice extent. The strongest anomalies were observed in the LS which experienced the most northerly sea-ice shift since satellite observations began in 1979 (National Snow and Sea Ice Data Center, NSIDC. http://nsidc.org/data). Unpublished data). In general, sea-ice displayed a strong gradient over the study region going from ice-free conditions in the outer LS to ice-dominated waters in the outer ESS (Fig.1.) Three snapshots of the sea-ice extent and concentrations (.i.e. at the beginning, in the middle and at the end of the sampling) is shown in Fig.1. Furthermore, Table 1 reports the averaged sea-ice concentrations encountered during the collection of each sample.

The surface water salinity exhibited a longitudinal trend characterized by low values in the outer LS while the sea-ice dominated ESS waters showed relatively higher values (Fig. 2a; Table 2). However, the highest salinity values were measured in the westernmost stations resulting in a sharp gradient in the LS. The low surface water salinities in the outer LS are most likely the result of both Lena river input and sea-ice thawing (Humborg et al., 2017) that started in late May (Janout et al., 2016).

9

225 The highest DOC concentrations were measured in the mid-outer LS in the surface

226 water plume affected by Lena River runoff (Fig.2b; Table 2). Overall, DOC concentrations

227 followed the plume dispersion with high DOC concentrations corresponding to low salinities

228 (Fig. 2). Carbon stable isotopes ($\delta^{13}C$) and terrestrial biomarkers (of the solid-phase extracted

229 DOC fraction; Salvado et al., 2016) further confirmed the influence of terrestrial DOC in the

230 outer LS, while the land-derived input progressively decreased moving eastward.

231 CO_2aq concentrations exhibited a typical estuarine pattern over the study region

232 (Humborg et al., 2017) (Fig. 2d; Table 2). Low salinity waters in the outer LS showed above

233 atmospheric CO_2 concentrations (i.e., oversaturation) while surface waters below sea-ice

234 exhibited undersaturated concentrations. The most depleted $\delta^{13}C_{CO2}$ values were measured off

235 the Lena river mouth (Fig. 2e; Table 2). Being relatively rich in land-derived material, it is

236 likely that respired terrestrial OC within the Lena river plume exerted control on the CO_2

237 isotopic signature and concentration (Humborg et al., 2017).

238 Finally, nutrient distribution revealed nitrate (NO_3) and nitrite (NO_2) depletion in

239 surface waters throughout the cruise track (Humborg et al., 2017) in comparison with the

240 Arctic Ocean gateways such as the Bering strait. Here, nutrient concentrations in surface

241 waters are two-order of magnitude higher compared the our study region (Torres-Valdés et

242 al., 2013). Phosphate (PO_4) exhibited rather low concentrations in the outer LS and relatively

243 higher concentrations below the sea-ice in the outer ESS (Humborg et al., 2017) likely

244 reflecting the inflow of nutrient-rich Pacific waters (Anderson et al., 2011; Semiletov et al.,

245 2005; Torres-Valdés et al., 2013).

246

247 **5. Results and discussion**

248 **5.1 Source of the POM (>10 μm) fraction**

249   The Arctic Ocean off northern Siberia receives large quantities of dissolved and

250   particulate terrestrial organic carbon via continental runoff and coastal erosion (Alling et al.,

251   2010; Dittmar and Kattner, 2003; McClelland et al., 2016; Sánchez-García et al., 2011;

252   Semiletov et al., 2013; Vonk et al., 2012). The land-derived material that does not settle in the

253   coastal zone further travels across the continental margin reaching out to the outer-shelf

254   region resuspended within the benthic nepheloid layer or in suspension within the surface

255   river plume (Fichot et al., 2013; Sánchez-García et al., 2011; Wegner et al., 2003). Another

256   fraction of terrestrial material can travel across the Siberian margin trapped in fast ice

257   (Dethleff, 2005). Considering the potential allochthonous contribution, we addressed to what

258   extent terrestrial organic material affects the POM (>10μm) fraction by quantifying the

259   concentration of lignin phenols and C16-18 hydroxy fatty acids (cutin-derived products).

260   These biomarkers are exclusively formed by terrestrial vegetation and, thus, serve as tracers

261   of land-derived material in the marine environment (Amon et al., 2012; Bröder et al., 2016b;

262   Feng et al., 2015).

263   Upon CuO alkaline oxidation the POM (>10μm) samples yielded only traces of lignin

264   phenols while the cutin-derived products were not detected (Fig. 3). Other oxidation products

265   in high abundance included saturated and mono-unsaturated short chain fatty acids (C12-

266   18FA), para-hydroxy phenols, benzoic acids and dicarboxylic acids. These other reaction

267   products are ubiquitous in both marine and terrestrial environments but they are predominant

268   in plankton-derived material, especially short-chain fatty acids (Goñi and Hedges, 1995).

269   When compared with active-layer permafrost soils and ice-complex deposits (Tesi et al.,

270   2014), POM (>10μm) samples displayed a distinct CuO fingerprint dominated by short chain

271   fatty acids (Fig. 3), consistent with the typical CuO products yields by phytoplankton batch

272   cultures upon CuO alkaline oxidation (Goñi and Hedges, 1995). SEM images further

273   corroborated the abundance of marine plankton detritus in the POM ($>10\mu m$) fraction while

274   lithogenic particles (clastic material) appeared to be sporadic in all samples.

275   The OC content (% d.w.) of the POM ($>10um$) fraction decreased eastwards showing

276   high concentrations in the LS and relatively low values in the ESS (Table 1; $p<0.01$ T-test).

277   However, in terms of absolute concentration in the water column ($\mu C/l$), the highest levels

278   were generally observed in the sea-ice covered region (Table 1; Fig. 4a; $p<0.01$ T-test).

279   Qualitative analyses by SEM and transmitted-light microscopy highlight important

280   differences in plankton assemblages which reflect different timing of the plankton blooms

281   which can explain these differences in concentration. Specifically, the open-water LS stations

282   exhibited a low degree of plankton diversity and were largely dominated by a bloom of

283   heterotrophic dinoflagellate cysts (*Protoperidinium* spp) (Fig. 5a; Table 3). Moving towards

284   the ice-dominated regions, diatoms become the prevailing species. Dominant diatom genera

285   include *Chaetoceros spp.* (dominant diatom in several stations), *Thalassiosira spp.*,

286   *Rhizosolenia spp.*, *Coscinodiscus spp.*, *Asteromphalus spp.*, *Navicula spp.* as well as sea-ice

287   species such as *Fragilariopsis cylindrus* and *Fragilariopsis oceanica* (Fig. 5b,c; Table 3).

288   Moored optical sensors deployed in the LS shelf recorded the sea-ice retreat in 2014

289   and found no sign of pelagic under-ice blooms despite available nutrients while high

290   chlorophyll concentrations were detected immediately after the ice retreated in late May

291   (Janout et al., 2016). The ice-edge blooms lasted for about 2 weeks according to the high

292   resolution chlorophyll time-series (Janout et al., 2016). Thus, our post-bloom sampling in the

293   LS essentially captured an oligotrophic environment dominated by heterotrophic

294   dinoflagellate cysts (i.e, Protoperidinium spp) which likely fed on phytodetritus and river-

295   derived organic material. Such conditions are fairly consistent with the relatively low carbon

296   contents ($\mu gC/L$) observed in LS waters (Fig. 4a).

297   The Arctic sea-ice biomarker IP25 (Fig. 4b) further highlight the different regimes

298   observed in ice-free and ice-dominated surface waters. IP25 is a proxy of sea-ice based on a

299   highly branched mono-unsaturated isoprenoid alkene found in some sea-ice diatoms which,

300   however, generally account for 5% of the total sea-ice taxa (Belt et al., 2007; Brown et al.,

301   2014b). The IP25 concentrations varied by several orders of magnitude over the study area

302   showing low concentrations in the open-water western region while the sea-ice dominated

303   surface waters to the east exhibited high concentrations especially at station 31b (Fig. 4b;

304   Table 1) ; $p<0.01$ Welch T-test). The fact that IP25 was still detectable throughout the ice-free

305   outer LS suggests that the proxy captured the signal of the sea-ice retreat that occurred shortly

306   before the sampling at the end of May/early June (Janout et al., 2016). Alternatively, the IP25

307   could have been advected from nearby sea-ice dominated regions.

308

309   **5.2. Dual carbon isotopes: δ^{13}C and Δ^{14}C**

310   δ^{13}C and Δ^{14}C of the POM (>10µm) samples exhibited a distinctive longitudinal trend

311   across the study area between LS and ESS (Fig. 4c,d) ($p<0.01$ T-test) . Depleted δ^{13}C values

312   characterized the LS open waters ranging from -28.1 to -24.7‰ (Fig. 4c). Although within the

313   range of terrestrially-derived material, our CuO oxidation data (i.e. trace of lignin phenols and

314   absence of cutin-derived products) suggest that the "light" isotopic composition in the LS

315   might instead reflect the plankton assemblage dominated by heterotrophic dinoflagellate cysts

316   as previously described (e.g., *Protoperidinium* spp; Fig. 5a). More specifically, heterotrophic

317   dinoflagellates can adapt their metabolism depending on the substrate available (e.g., diatoms

318   and bacteria). Several studies have shown that terrestrial DOC greatly promotes bacteria

319   biomass production which in turn stimulates the growth of heterotrophic dinoflagellates

320   (Carlsson et al., 1995; Purina et al., 2004; Wikner and Andersson, 2012). Thus, in these

321   conditions, allochthonous terrestrial DOC is actively recycled by bacteria and transferred to

322   dinoflagellates which explains, thus, the depleted $\delta^{13}C$ values observed in the river-dominated

323   samples (Carlsson et al., 1995).

324   The modern radiocarbon fingerprint of the Lena DOC discharge is consistent with

325    $\Delta^{14}C$ signature of the POM (>10μm) fraction in the LS (up to +99 ‰), supporting the

326   importance of terrestrial DOC as a carbon source for the food web in the river plume (Fig. 4d

327   and 6). By contrast, comparison with other potential carbon sources which include the Lena

328   river particulate organic carbon, surface sediments, Pleistocene coastal Ice-Complex Deposit

329   and Pacific DIC inflow reveals a different (more depleted) radiocarbon fingerprint (Fig. 6). It

330   is also import to highlight that the DOC within the Lena plume is one/two-order of magnitude

331   higher than the particulate carbon pool supporting, thus, our hypothesis (Humborg et al.,

332   2017; Salvadó et al., 2016).

333   Moving towards the ice-dominated ESS, surface waters progressively become more

334   autotrophic and productive (Humborg et al., 2017) while the POM (>10μm) exhibited a wide

335    $\delta^{13}C$ signature ranging from -28.6 to -21.2‰ (Fig. 4c). The most depleted values were

336   observed across the transition zone between open-waters and sea-ice. Visual inspections of

337   these samples revealed large abundance of the centric diatom *Chaetoceros* spp. (spores and

338   vegetative cells; St22, Fig. 5b) while lignin and cutin data indicated, a negligible input of

339   land-derived material. Primary factors determining the fractionation of stable carbon isotopes

340   in phytoplankton are several and include CO_2aq concentration, $\delta^{13}Caq$, growth rate, cell size,

341   cell shape, light and nutrient availability (Gervais and Riebesell, 2001; Laws et al., 1997a;

342   Popp et al., 1998; Rau et al., 1996). Our understanding about isotopic fractionation has been

343   historically achieved via laboratory experiments designed to test each factor under controlled

344   conditions. In natural environments, however, different factors can compete with each other,

345   sometimes in opposite directions. Yet, the existing knowledge about surface water properties

346 during the expedition (Humborg et al., 2017) can provide important constraints for the

347 isotopic signal interpretation.

348 For example, comparison with continuous δ^{13}C-CO$_2$aq and CO$_2$aq data measured

349 throughout the cruise track - time-averaged to match the large volume filtration along the

350 cruise track (Table 1) - suggested a negligible role exerted by δ^{13}C-CO$_2$aq (Fig. 7b) while

351 CO$_2$aq concentration correlated with the δ^{13}C of the POM (>10μm) fraction (r^2=0.72; *p*<0.01)

352 (Fig. 7a). Such a relationship fits with the general model according to which a low demand

353 (i.e., low growth rate) and high supply (i.e., abundant CO$_2$aq) favour high fractionation and

354 vice versa (Laws et al., 1997b; Laws et al., 1995; Wolf-Gladrow et al., 1999).

355 During the expedition, surface water properties (i.e. O$_2$ and CO$_2$, Table 2) (Humborg

356 et al., 2017) suggest that the productivity in the outer ESS increases moving eastward, as

357 commonly observed, likely due to the Pacific inflow (Björk et al., 2011; Semiletov et al.,

358 2005). As a result, the wide range of plankton δ^{13}C over the ESS can be explained in terms of

359 two different regimes: (a) in the transition zone between open waters and sea-ice, the

360 productivity was low but CO$_2$aq was oversaturated while (b) in the easternmost ESS,

361 productivity was high but CO$_2$aq was depleted (Fig. 7b). The former regime favours

362 fractionation while the latter does not (Fig. 7b). Different diatom assemblages can also be

363 another factor to consider although the phytoplankton diversity observed over ESS can be

364 considered rather small (e.g. *Chaetoceros spp.* dominant in most of the samples) compared to

365 the wide range of δ^{13}C observed (i.e., from -28.8 to -21.6) (Table 3).

366 The POM (>10μm) fraction in the sea-ice dominated ESS exhibited slightly - but

367 consistently - depleted Δ^{14}C values ranging from -62 to -49 ‰ (Fig. 4d). This region is

368 affected by the inflow of Pacific waters whose DIC exhibits, however, a modern Δ^{14}C

369 signature (Griffith et al., 2012) (Fig. 6). By contrast, these results suggest the influence from

370 an aged carbon pool. As the ESS remains covered by sea-ice for most of the year, it is

371 possible that the sea-ice hampers the gas exchange with the atmosphere and acts as a lid by

372 trapping CO_2 which derives from the breakdown of sedimentary organic material (Anderson

373 et al., 2009; Semiletov et al., 2016), which might have such ages (Bröder et al., 2016a; Vonk

374 et al., 2012). In these conditions, the pre-aged CO_2 accumulates underneath the sea-ice and is

375 subsequently incorporated during carbon fixation by the phytoplankton. While oversaturated

376 bottom waters were extensively documented in the region with important consequences on the

377 local DIC (Anderson et al., 2009; Pipko et al., 2009), more work is clearly needed to

378 understand if early diagenesis in sediments can also affect the radiocarbon signature of the

379 CO_2aq underneath the sea-ice. Alternatively, the slightly depleted radiocarbon signature might

380 indicate the presence of pre-aged terrestrial organic carbon (Fig. 6) in the POM (>10μm)

381 samples, not reflected in the lignin and cutin tracers (Fig. 3). However, it would then remain

382 elusive why such an aged land-derived influence was not visible in the river-dominated LS

383 waters while it affected the sea-ice dominated region.

384 Taken together, our results indicate that the dual-carbon isotope fingerprint is highly

385 affected by the trophic conditions (heterotrophic *vs* autotrophic) as well as the extent of

386 primary productivity. In a warming scenario characterized by sea-ice retreat (Arrigo et al.,

387 2008; Comiso et al., 2008) and enhanced terrestrial input from land as result of hydrology and

388 permafrost destabilization (Frey and Smith, 2005; Vonk et al., 2012), the geochemical

389 composition of plankton will likely change as the warming proceeds.

390

6. Conclusions

392 Analyses of large-volume filtrations of plankton-dominated >10 μm particle samples

393 revealed a high degree of heterogeneity in the dual carbon isotope signature ($\delta^{13}C$ and $\Delta^{14}C$)

394 between ice-free waters (Laptev Sea) and the ice-covered region (East Siberian Sea).

395   Our results suggest a heterotrophic environment in the outer LS open waters where the

396    $\delta^{13}C$ depleted river DOC is transferred to relatively higher trophic levels via microbial

397   incorporation in the river plume. Moving eastwards towards the ice-dominated outer ESS,

398   surface waters became progressively more autotrophic. Here, the isotopic fractionation

399   appears to follow the phytoplankton growth *vs* CO_2 demand model according to which carbon

400   fractionation decreases at high growth and low CO_2 concentrations. As a result, the transition

401   between open-waters and sea-ice exhibited more depleted $\delta^{13}C$ values compared to the

402   productive easternmost stations. Radiocarbon signatures were slightly depleted over the whole

403   sea-ice dominated area. This raises the question whether the sea-ice hampers the gas exchange

404   with the atmosphere and trap the CO_2 sourced from reactive sedimentary carbon pools.

405   In a warming scenario, it is likely that the oligotrophic ice-free LS will be dominated

406   by heterotrophic metabolism fuelled by terrestrially-derived organic material (i.e., Lena

407   input). In these conditions, the dual-carbon isotope signature of the heterotrophic plankton

408   will essentially reflect the terrestrial fingerprint. In the ESS, which receives the inflow of the

409   nutrient-rich Pacific waters, ice-free conditions will enhance light penetration. This in turn

410   might further stimulate phytoplankton growth with important implications in terms of CO_2

411   depletion and resulting low isotope fractionation. Altogether, this will result in a sharp

412   compositional gradient (e.g. $\delta^{13}C$) between LS and ESS similar to what captured in our semi-

413   synoptic study.

414

428

429

430

431

432

433

434

435

436

437

438

439

440

441

442

443

444

Table 1. Chemical composition of the POM (>10μm) fraction and continuous CO₂aq measurements*

ID	Time averaged latitude (N)	Time averaged longitude (E)	Mean sea-ice percentage (%)	POM (>10μm) concentration (mg/l)	OC (d.w.)	$\delta^{13}C$ (‰)	$\Delta^{14}C$ (‰)	IP25 (ng/gOC)	averege CO₂aq (ppm)*	average $\delta^{13}C$-CO₂aq (‰)*
ST4	81.68	105.96	98.4	6	18.2	-26.7	n.d.	n.d.	323	-10.9
ST5	80.47	114.07	98.7	15	42.6	-27.6	n.d.	n.d.	322	-11.0
ST6	78.86	125.22	82.2	1	51.7	-26.6	99	n.d.	325	-10.8
ST7	77.88	126.62	0.0	11	43.1	-25.7	n.d.	88	350	-10.7
ST8	77.16	127.32	0.0	17	30.9	-26.7	41	n.d.	391	-10.5
ST9	76.78	125.83	0.0	3	31.5	-27.9	30	48	385	-10.5
ST10	76.90	127.81	0.0	11	40.9	-24.7	n.d.	n.d.	349	-11.0
ST11	77.12	126.66	0.0	13	29.6	-28.1	27	13	428	-10.7
ST22	77.67	144.63	0.0	20	11.3	-28.8	n.d.	95	394	-11.0
ST23	76.43	147.53	0.0	6	7.6	-28.5	-50	n.d.	394	-11.2
ST24	76.42	149.84	34.4	19	11.9	-26.8	-62	368	374	-11.1
ST25	76.62	152.03	96.7	23	19.5	-25.7	-31	465	263	-10.8
ST26	76.14	157.85	96.2	109	30.8	-24.2	-30	217	316	-10.9
ST27	75.00	161.03	91.5	41	23.3	-23.0	n.d.	256	299	-11.1
ST28	74.63	161.98	86.3	28	15.5	-23.8	n.d.	n.d.	214	-11.3
ST29	73.61	169.72	79.3	31	14.7	-23.2	-50	518	184	-11.3
ST30	75.61	174.01	66.7	43	22.6	-27.0	n.d.	n.d.	304	-10.5
ST31A	75.85	174.41	75.6	30	10.9	-21.6	-62	1911	182	-10.6
ST31B	74.26	173.74	63.5	15	4.6	-23.3	n.d.	783	n.d.	n.d.
ST32	73.56	176.06	51.8	21	11.3	-24.5	-58	131	n.d.	n.d.
ST33	72.35	-175.14	0.0	20	15.5	-23.5	n.d.	473	n.d.	n.d.
ST34	73.28	-173.05	28.7	76	13.4	-21.6	-52	970	n.d.	n.d.
ST35	75.21	-172.05	53.9	24	14.3	-24.2	n.d.	268	n.d.	n.d.

n.d = not determined
*Humborg et al. (2017)

446

447

448

449

450

451

452

453

454

455

Table 2. Surface water (0-20 m) chemical and physical properties during the SWERUS-C3 expedition*

	Salinity	Temperature	DIC	DOC	POC	δ^{13}C-DIC	NO$_2$-NO$_3$	PO$_4$	O$_2$
		°C	µmol kg^{-1}	µmol kg^{-1}	µmol kg^{-1}	‰	µmol kg^{-1}	µmol kg^{-1}	µmol kg^{-1}
	median	median	median	median	median	median	median	median	median
Outer LS shelf (0-20 m)	32.87	3.84	2139	149.1	7.9	0.75	0.21	0.27	323.0
LS shelf break (0-20 m)	33.56	0.57	2114	91.5	10.1	1.10	0.26	0.15	364.9
Outer ESS shelf (0-20 m)	29.45	-1.33	1969	84.2	10.7	1.14	0.25	0.97	381.5
ESS shelf break (0-20 m)	28.23	-1.32	1979	73.7	4.6	1.47	0.11	0.59	394.1
	mean	mean	mean	mean	mean	mean	mean	mean	mean
Outer LS shelf (0-20 m)	31.17	3.40	2119	179.8	7.9	0.58	0.60	0.29	327.0
LS shelf break (0-20 m)	33.42	0.96	2111	97.5	10.0	1.10	0.61	0.16	358.1
Outer ESS shelf (0-20 m)	28.95	-0.05	1949	95.8	11.9	1.26	0.26	0.95	386.8
ESS shelf break (0-20 m)	28.27	-1.31	1975	72.0	4.6	1.49	0.12	0.60	397.0
	s.d.	s.d.	s.d.	s.d.	s.d.	s.d.	s.d.	s.d.	s.d.
Outer LS shelf (0-20 m)	3.22	2.38	89	66.3	1.7	0.50	0.91	0.11	14.6
LS shelf break (0-20 m)	0.70	2.07	23	21.2	1.7	0.11	0.74	0.06	22.5
Outer ESS shelf (0-20 m)	1.41	2.28	75	30.2	4.6	0.49	0.12	0.19	32.2
ESS shelf break (0-20 m)	0.53	0.04	49	3.2	0.3	0.08	0.03	0.02	8.3

*data from Humborg et al. (2017) and Salvadó et al. (2016)

456

457

458

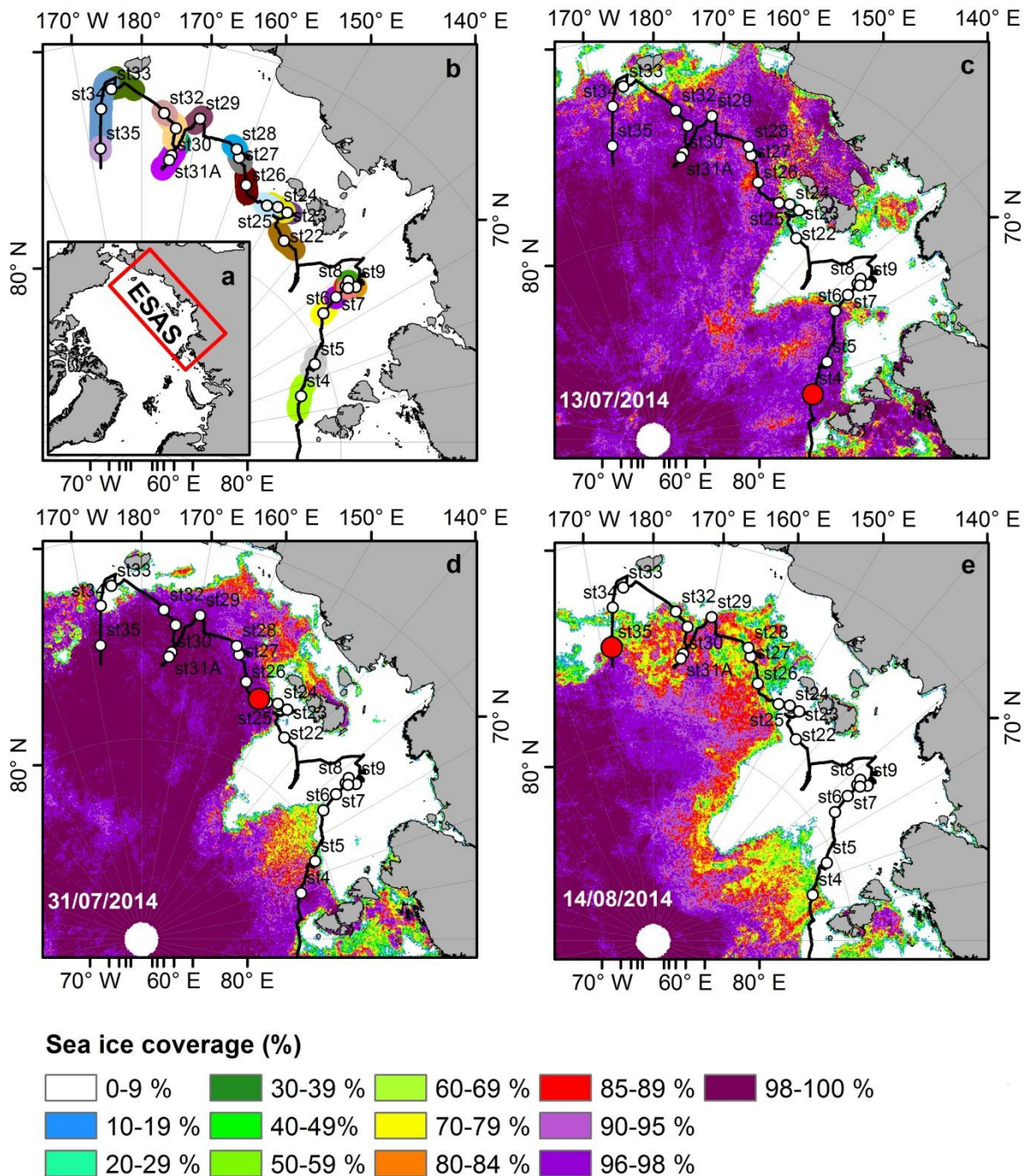459

460

461

462

463

464

465

466

467

468

469

**Table 3. Qualitative plankton characterization of selected POM (>10μm) samples**

ID	Region	Diatoms	Dinoflagellates	Other species
ST6	LS	Few *Coscinodiscus*	None observed	
ST9	LS	None observed	Few *Protoperidinium*	
ST11	LS	None observed	Abundant *Protoperidinium*	
ST22	LS-ESS	Abundant *Chaetoceros*, few *Rhizosolenia*, *Thalassiosira*	None observed	
ST25	LS-ESS	High diversity. Abundant *Chaetoceros, few Rhizosolenia, Coscinodiscus, Thallasiosira, Asteromphalus, Navicula*	None observed	Silicoflagellate
ST31A	ESS	High diversity. Abundant *Chaetoceros, few Rhizosolenia, Thallasiosira, Bacterosira, Navicula*	None observed	
ST31B	ESS	High diversity. Few *Chaetoceros, Thallasiosira, Fragilariopsis*	Few *Protoperidinium*	
ST34	ESS	Abundant *Chaetoceros*, few *Thalassiosira, Navicula*	Few *Protoperidinium*	

470

471

472

473

474

475

476

477

478

479

480

481

482

483

484

485

486

Fig. 1 (a) The study area in the East Siberian Arctic Shelf. (b) Time-averaged position during the large-volume filtration (circles) of the POM (>10μm) samples. Shaded coloured areas show the sampling area covered to harvest each POM (>10μm) sample. Sea-ice extent and concentration at the beginning (c), in the middle (d) and at the end (e) of the sampling campaign. The ship position is shown by a filled red circle.
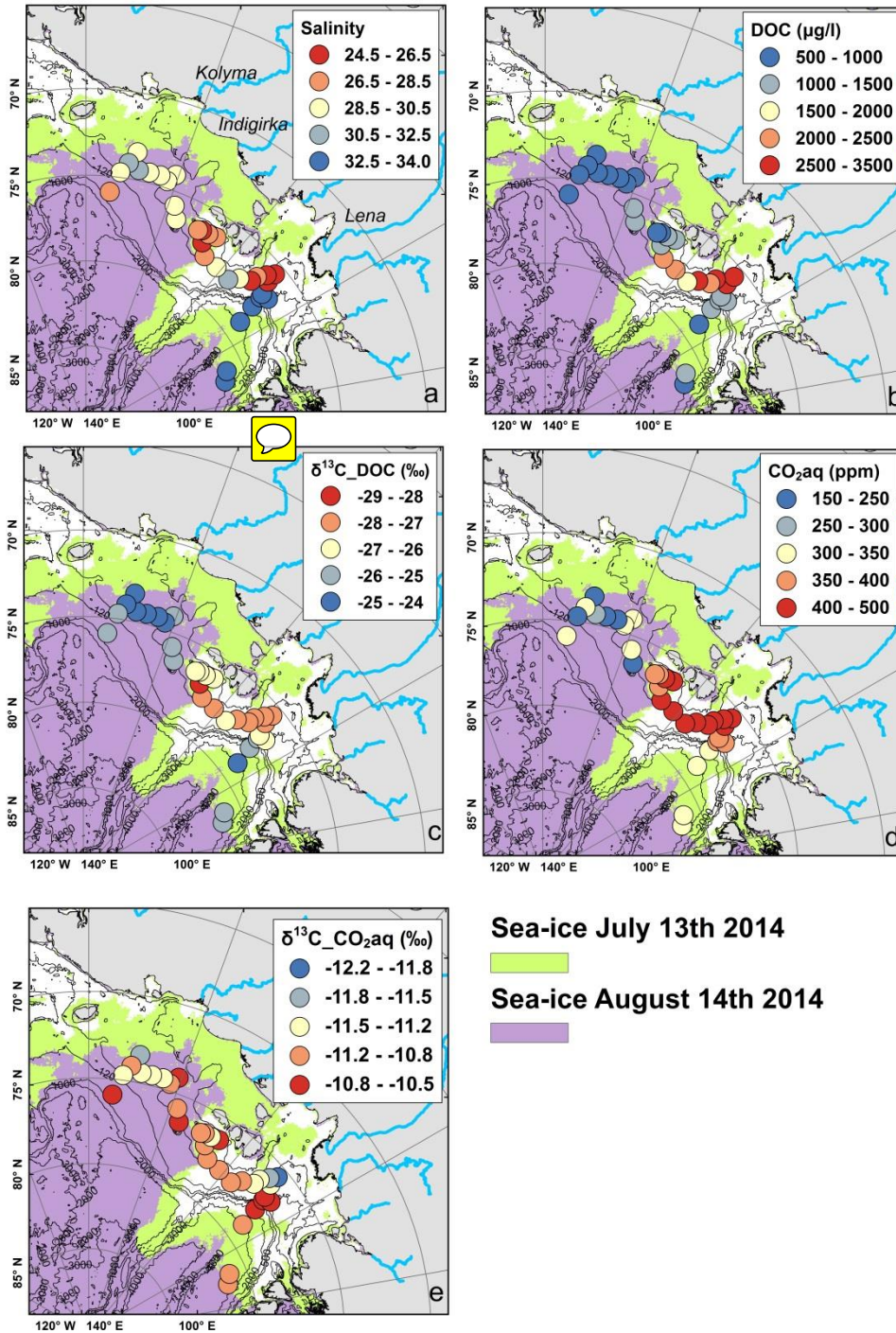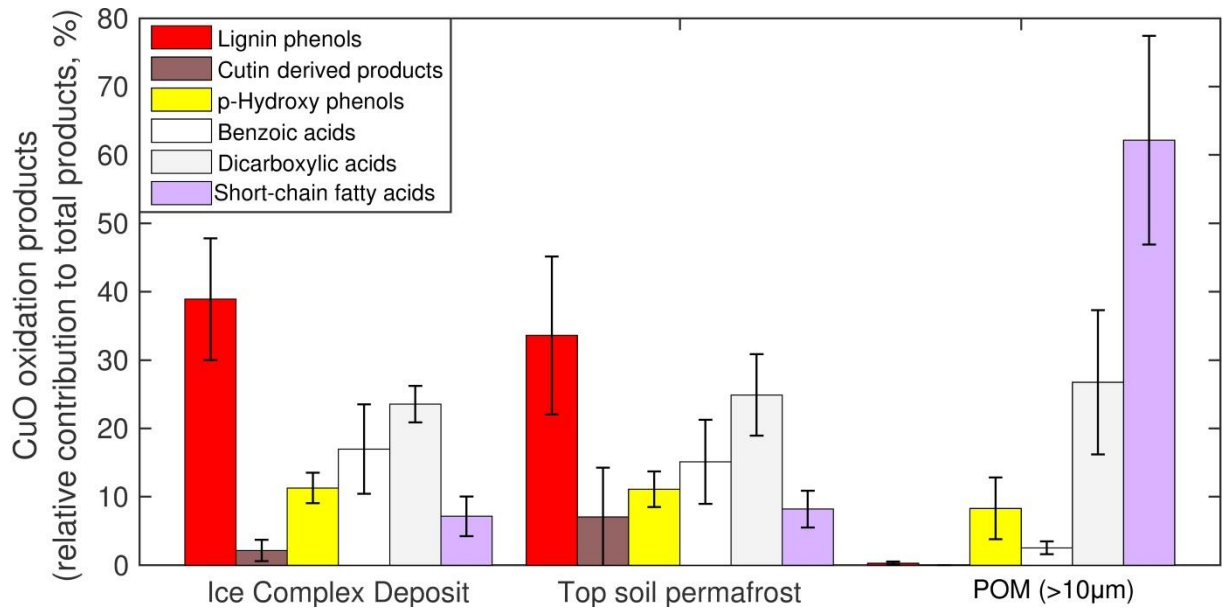
Fig.2 Surface water properties. (a) Salinity. (b) DOC. (c) δ^{13}C-DOC. (d) CO_2aq. (e) δ^{13}C-CO_2aq. Shaded areas show the sea-ice extent at the beginning (13/07/2014) and at the end of the sampling campaign (14/08/2014) (Humborg et al., 2017; Salvadó et al., 2016).

23

Fig.3 Alkaline CuO fingerprint of top-soil permafrost samples (Tesi et al., 2014), Pleistocene Ice Complex Deposit (Tesi et al., 2014) and POM (>10μm) fraction (this study). The plot displays the relative proportion products yield upon alkaline CuO oxidation. The error bar refers to the natural variability of each dataset

POM (>10 μm) samples
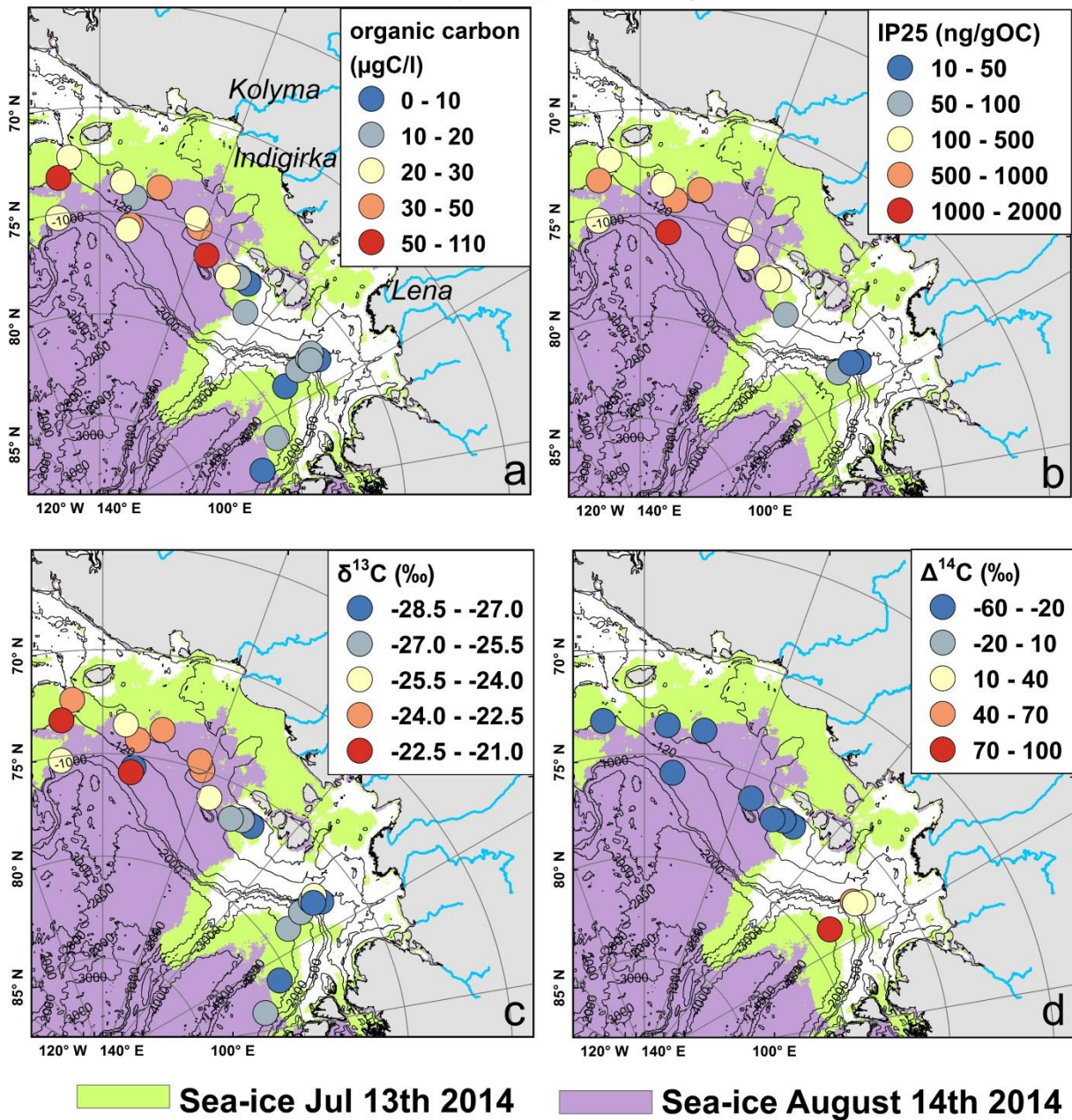
Fig. 4 POM (>10μm) composition (a) Organic carbon concentration. (b) IP25 (mono-unsaturated highly branched isoprenoid. (c) δ¹³C. (d) Δ¹⁴C. Shaded areas show the sea-ice extent at the beginning (13/07/2014) and at the end of the sampling campaign (14/08/2014).
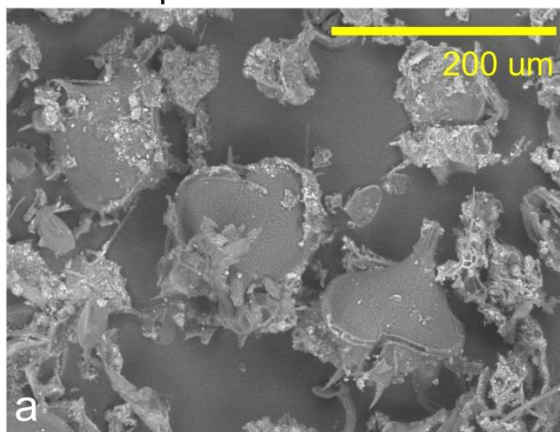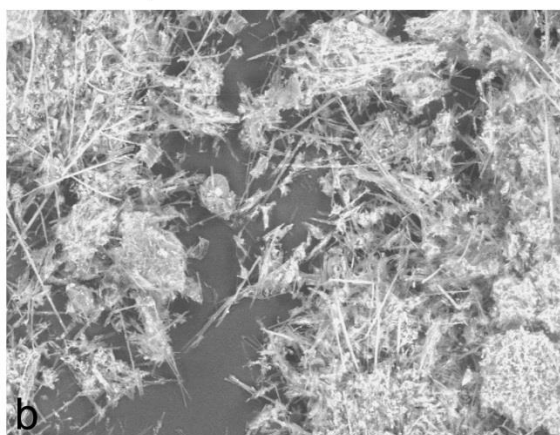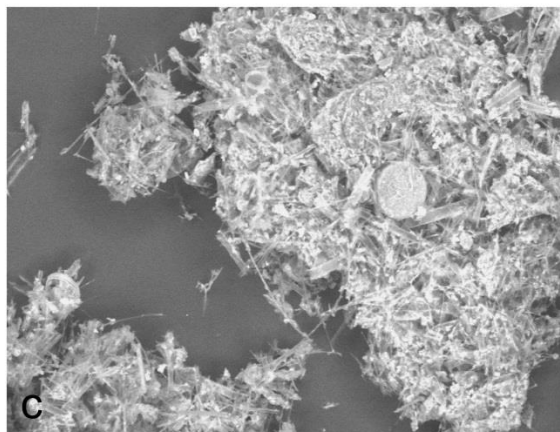
ST11 - Laptev Sea
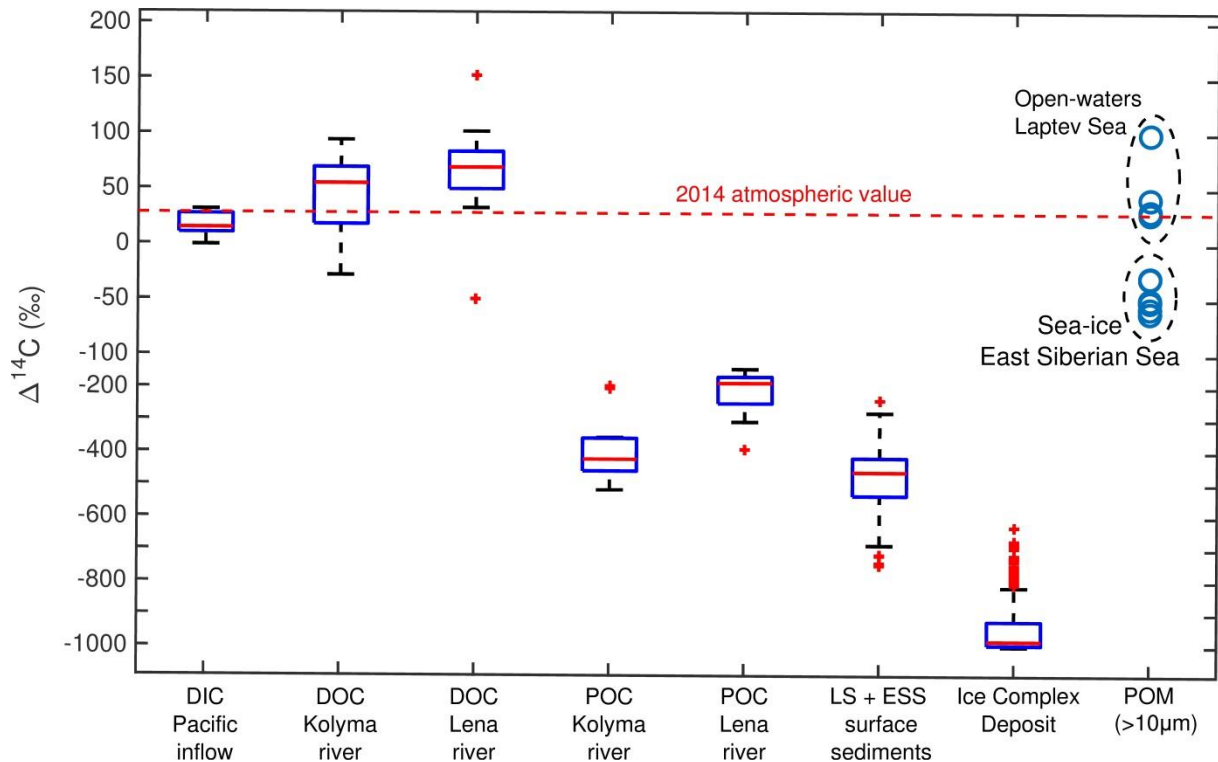

ST22 - Laptev Sea / East Siberian Sea

ST34 - East Siberian Sea

524

525

Fig. 5 SEM images. (a) ST-11: Dinoflagellates (*Protoperidinium* spp.) in open-waters of the Laptev Sea. (b) ST22: Diatoms, mostly spines (setae) of *Chaetoceros* spp. in the transition between Laptev Sea and East Siberian Sea. (c) ST-34: Diatoms from sea-ice dominated waters in the East Siberian Sea

Fig. 6 Radiocarbon signature of inorganic and organic carbon pools. Whisker plots of

radiocarbon values for different inorganic and organic carbon sources from the literature,

compared to the outer Laptev Sea and outer East Siberian Sea (blue circles, this study). Solid

lines show the median, the box limits display the 25th and 75th percentiles while the crosses

show the outliers. Source: DIC (Griffith et al., 2012), DOC-Kolyma (2009-2014), DOC-Lena

(2009-2014), POC-Kolyma (2009-2011), POC-Lena (2009-2011)

(www.arcticgreatrivers.org), Laptev Sea and Eastern Siberia Sea surface sediments (Salvadó

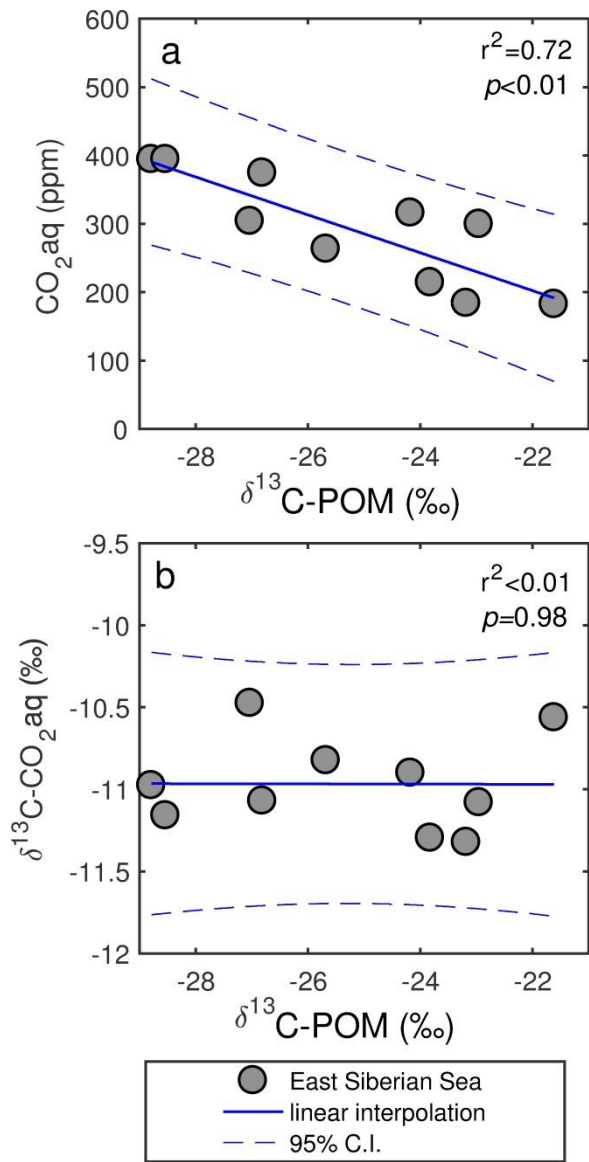et al., 2016; Vonk et al., 2012) and Ice Complex Deposit (Vonk et al., 2012).

Fig. 7 Correlations (a) CO_2aq vs $\delta^{13}C$ (POM (>10μm) fraction) and (b) $\delta^{13}C$-CO_2aq vs $\delta^{13}C$ in the East Siberian Sea (filled circles). The solid line shows the linear interpolation while the dashed line shows the 95% confidence intervals.

References

556 **References**

557 Aagaard, K. and Carmack, E. C.: The role of sea ice and other fresh water in the Arctic circulation,
558 Journal of Geophysical Research: Oceans, 94, 14485-14498, 1989.

559 Alling, V., Sanchez-Garcia, L., Porcelli, D., Pugach, S., Vonk, J. E., van Dongen, B., Mörth, C.-M.,
560 Anderson, L. G., Sokolov, A., Andersson, P., Humborg, C., Semiletov, I., and Gustafsson, Ö.:
561 Nonconservative behavior of dissolved organic carbon across the Laptev and East Siberian seas,
562 Global Biogeochemical Cycles, 24, n/a-n/a, 2010.

563 Amon, R., Rinehart, A., Duan, S., Louchouarn, P., Prokushkin, A., Guggenberger, G., Bauch, D.,
564 Stedmon, C., Raymond, P., and Holmes, R.: Dissolved organic matter sources in large Arctic rivers,
565 Geochimica et Cosmochimica Acta, 94, 217-237, 2012.

566 Anderson, L. G., Björk, G., Jutterström, S., Pipko, I., Shakhova, N., Semiletov, I., and Wåhlström, I.:
567 East Siberian Sea, an Arctic region of very high biogeochemical activity, Biogeosciences, 8, 1745-
568 1754, 2011.

569 Anderson, L. G., Jutterström, S., Hjalmarsson, S., Wåhlström, I., and Semiletov, I.: Out-gassing of CO2
570 from Siberian Shelf seas by terrestrial organic matter decomposition, Geophysical Research Letters,
571 36, 2009.

572 Ardyna, M., Babin, M., Gosselin, M., Devred, E., Rainville, L., and Tremblay, J. É.: Recent Arctic Ocean
573 sea ice loss triggers novel fall phytoplankton blooms, Geophysical Research Letters, 41, 6207-6212,
574 2014.

575 Arrigo, K. R., van Dijken, G., and Pabi, S.: Impact of a shrinking Arctic ice cover on marine primary
576 production, Geophysical Research Letters, 35, n/a-n/a, 2008.

577 Belt, S. T., Brown, T. A., Rodriguez, A. N., Sanz, P. C., Tonkin, A., and Ingle, R.: A reproducible method
578 for the extraction, identification and quantification of the Arctic sea ice proxy IP25 from marine
579 sediments, Analytical Methods, 4, 705-713, 2012.

580 Belt, S. T., Massé, G., Rowland, S. J., Poulin, M., Michel, C., and LeBlanc, B.: A novel chemical fossil of
581 palaeo sea ice: IP25, Organic Geochemistry, 38, 16-27, 2007.

582 Björk, G., Jutterström, S., Pipko, I., Shakhova, N., Semiletov, I., and Wåhlström, I.: East Siberian Sea,
583 an Arctic region of very high biogeochemical activity, Biogeosciences, 8, 1745, 2011.

584 Bröder, L., Tesi, T., Andersson, A., Eglinton, T. I., Semiletov, I. P., Dudarev, O. V., Roos, P., and
585 Gustafsson, Ö.: Historical records of organic matter supply and degradation status in the East
586 Siberian Sea, Organic Geochemistry, 91, 16-30, 2016a.

587 Bröder, L., Tesi, T., Salvadó, J. A., Semiletov, I. P., Dudarev, O. V., and Gustafsson, Ö.: Fate of
588 terrigenous organic matter across the Laptev Sea from the mouth of the Lena River to the deep sea
589 of the Arctic interior, Biogeosciences, 13, 5003-5019, 2016b.

590 Brown, T. A., Belt, S. T., Tatarek, A., and Mundy, C. J.: Source identification of the Arctic sea ice proxy
591 IP25, 5, 4197, 2014a.

592 Brown, T. A., Belt, S. T., Tatarek, A., and Mundy, C. J.: Source identification of the Arctic sea ice proxy
593 IP25, Nature Communications, 5, 4197, 2014b.

594 Carlsson, P., Graneli, E., Tester, P., and Boni, L.: Influences of riverine humic substances on bacteria,
595 protozoa, phytoplankton, and copepods in a coastal plankton community, Marine Ecology Progress
596 Series, 127, 213-221, 1995.

597 Comiso, J. C., Parkinson, C. L., Gersten, R., and Stock, L.: Accelerated decline in the Arctic sea ice
598 cover, Geophysical research letters, 35, 2008.

599 Dethleff, D.: Entrainment and export of Laptev Sea ice sediments, Siberian Arctic, Journal of
600 Geophysical Research: Oceans, 110, n/a-n/a, 2005.

601 Ding, Q., Schweiger, A., Lheureux, M., Battisti, D. S., Po-Chedley, S., Johnson, N. C., Blanchard-
602 Wrigglesworth, E., Harnos, K., Zhang, Q., Eastman, R., and Steig, E. J.: Influence of high-latitude
603 atmospheric circulation changes on summertime Arctic sea ice, Nature Clim. Change, 7, 289-295,
604 2017.

Dittmar, T. and Kattner, G.: The biogeochemistry of the river and shelf ecosystem of the Arctic Ocean: a review, Marine chemistry, 83, 103-120, 2003.

Dunton, K. H., Weingartner, T., and Carmack, E. C.: The nearshore western Beaufort Sea ecosystem: Circulation and importance of terrestrial carbon in arctic coastal food webs, Progress in Oceanography, 71, 362-378, 2006.

Feng, X., Gustafsson, Ö., Holmes, R. M., Vonk, J. E., van Dongen, B. E., Semiletov, I. P., Dudarev, O. V., Yunker, M. B., Macdonald, R. W., Wacker, L., Montluçon, D. B., and Eglinton, T. I.: Multimolecular tracers of terrestrial carbon transfer across the pan-Arctic: 14C characteristics of sedimentary carbon components and their environmental controls, Global Biogeochemical Cycles, 29, 1855-1873, 2015.

Fichot, C. G., Kaiser, K., Hooker, S. B., Amon, R. M., Babin, M., Bélanger, S., Walker, S. A., and Benner, R.: Pan-Arctic distributions of continental runoff in the Arctic Ocean, Scientific reports, 3, 1053, 2013.

Frey, K. E. and Smith, L. C.: Amplified carbon release from vast West Siberian peatlands by 2100, Geophysical Research Letters, 32, 2005.

Fujiwara, A., Hirawake, T., Suzuki, K., Imai, I., and Saitoh, S.-I.: Timing of sea ice retreat can alter phytoplankton community structure in the western Arctic Ocean, Biogeosciences, 11, 1705-1716, 2014.

Gervais, F. and Riebesell, U.: Effect of phosphorus limitation on elemental composition and stable carbon isotope fractionation in a marine diatom growing under different CO_2 concentrations, Limnology and Oceanography, 46, 497-504, 2001.

Goñi, M. A. and Hedges, J. I.: Potential applications of cutin-derived CuO reaction products for discriminating vascular plant sources in natural environments, Geochimica et Cosmochimica Acta, 54, 3073-3081, 1990.

Goñi, M. A. and Hedges, J. I.: Sources and reactivities of marine-derived organic matter in coastal sediments as determined by alkaline CuO oxidation, Geochimica et Cosmochimica Acta, 59, 2965-2981, 1995.

Gordeev, V. V.: Fluvial sediment flux to the Arctic Ocean, Geomorphology, 80, 94-104, 2006.

Griffith, D. R., McNichol, A. P., Xu, L., McLaughlin, F. A., Macdonald, R. W., Brown, K. A., and Eglinton, T. I.: Carbon dynamics in the western Arctic Ocean: insights from full-depth carbon isotope profiles of DIC, DOC, and POC, 2012. 2012.

Gustafsson, Ö., Andersson, P., Axelman, J., Bucheli, T., Kömp, P., McLachlan, M., Sobek, A., and Thörngren, J.-O.: Observations of the PCB distribution within and in-between ice, snow, ice-rafted debris, ice-interstitial water, and seawater in the Barents Sea marginal ice zone and the North Pole area, Science of the total environment, 342, 261-279, 2005.

Gustafsson, Ö. and Andersson, P. S.: 234Th-derived surface export fluxes of POC from the Northern Barents Sea and the Eurasian sector of the Central Arctic Ocean, Deep Sea Research Part I: Oceanographic Research Papers, 68, 1-11, 2012.

Hoins, M., Van de Waal, D. B., Eberlein, T., Reichart, G.-J., Rost, B., and Sluijs, A.: Stable carbon isotope fractionation of organic cyst-forming dinoflagellates: Evaluating the potential for a CO_2 proxy, Geochimica et Cosmochimica Acta, 160, 267-276, 2015.

Humborg, C., Geibel, M. C., Anderson, L. G., Björk, G., Mörth, C.-M., Sundbom, M., Thornton, B. F., Deutsch, B., Gustafsson, E., Gustafsson, B., Ek, J., and Semiletov, I.: Sea-air exchange patterns along the central and outer East Siberian Arctic Shelf as inferred from continuous CO_2, stable isotope and bulk chemistry measurements Global Biogeochemical Cycles, doi: 10.1002/2017GB005656, 2017. 2017.

Iken, K., Bluhm, B., and Gradinger, R.: Food web structure in the high Arctic Canada Basin: evidence from $\delta 13C$ and $\delta 15N$ analysis, Polar Biology, 28, 238-249, 2005.

Janout, M. A., Hölemann, J., Waite, A. M., Krumpen, T., Appen, W. J., and Martynov, F.: Sea-ice retreat controls timing of summer plankton blooms in the Eastern Arctic Ocean, Geophysical Research Letters, 2016. 2016.

Karlsson, E., Gelting, J., Tesi, T., Dongen, B., Andersson, A., Semiletov, I., Charkin, A., Dudarev, O., and Gustafsson, Ö.: Different sources and degradation state of dissolved, particulate and sedimentary organic matter along the Eurasian Arctic coastal margin, Global Biogeochemical Cycles, 2016. 2016.

657 Kohlbach, D., Graeve, M., A Lange, B., David, C., Peeken, I., and Flores, H.: The importance of ice
658 algae-produced carbon in the central Arctic Ocean ecosystem: Food web relationships revealed by
659 lipid and stable isotope analyses, Limnology and Oceanography, 2016. 2016.
660 Kwok, R. and Rothrock, D.: Decline in Arctic sea ice thickness from submarine and ICESat records:
661 1958–2008, Geophysical Research Letters, 36, 2009.
662 Lalande, C., Bélanger, S., and Fortier, L.: Impact of a decreasing sea ice cover on the vertical export of
663 particulate organic carbon in the northern Laptev Sea, Siberian Arctic Ocean, Geophysical Research
664 Letters, 36, n/a-n/a, 2009.
665 Lalande, C., Nöthig, E. M., Somavilla, R., Bauerfeind, E., Shevchenko, V., and Okolodkov, Y.: Variability
666 in under-ice export fluxes of biogenic matter in the Arctic Ocean, Global Biogeochemical Cycles, 28,
667 571-583, 2014.
668 Lantuit, H., Atkinson, D., Paul Overduin, P., Grigoriev, M., Rachold, V., Grosse, G., and Hubberten, H.-
669 W.: Coastal erosion dynamics on the permafrost-dominated Bykovsky Peninsula, north Siberia, 1951–
670 2006, Polar Research, 30, 7341, 2011.
671 Laws, E. A., Bidigare, R. R., and Popp, B. N.: Effect of growth rate and CO~ 2 concentration on carbon
672 isotopic fractionation by the marine diatom Phaeodactylum tricornutum, Limnology and
673 Oceanography, 42, 1552-1560, 1997a.
674 Laws, E. A., Bidigare, R. R., and Popp, B. N.: Effect of growth rate and CO~ 2 concentration on carbon
675 isotopic fractionation by the marine diatom Phaeodactylum tricornutum, 1997b. 1997b.
676 Laws, E. A., Popp, B. N., Bidigare, R. R., Kennicutt, M. C., and Macko, S. A.: Dependence of
677 phytoplankton carbon isotopic composition on growth rate and [CO2] aq: Theoretical considerations
678 and experimental results, Geochimica et cosmochimica acta, 59, 1131-1138, 1995.
679 McClelland, J. W., Holmes, R. M., Peterson, B. J., Raymond, P. A., Striegl, R., Zhulidov, A. V., Zimov, S.,
680 Zimov, N., Tank, S. E., and Spencer, R. G.: Particulate organic carbon and nitrogen export from major
681 Arctic rivers, Global Biogeochemical Cycles, 30, 629-643, 2016.
682 Nieuwenhuize, J., Maas, Y. E., and Middelburg, J. J.: Rapid analysis of organic carbon and nitrogen in
683 particulate materials, Marine Chemistry, 45, 217-224, 1994.
684 Pagani, M., Arthur, M. A., and Freeman, K. H.: Miocene evolution of atmospheric carbon dioxide,
685 Paleoceanography, 14, 273-292, 1999.
686 Pipko, I. I., Pugach, S. P., and Semiletov, I. P.: The autumn distribution of the CO2 partial pressure in
687 bottom waters of the East Siberian Sea, Doklady Earth Sciences, 425, 345-349, 2009.
688 Popp, B. N., Laws, E. A., Bidigare, R. R., Dore, J. E., Hanson, K. L., and Wakeham, S. G.: Effect of
689 phytoplankton cell geometry on carbon isotopic fractionation, Geochimica et cosmochimica acta, 62,
690 69-77, 1998.
691 Popp, B. N., Trull, T., Kenig, F., Wakeham, S. G., Rust, T. M., Tilbrook, B., Griffiths, B., Wright, S. W.,
692 Marchant, H. J., and Bidigare, R. R.: Controls on the carbon isotopic composition of Southern Ocean
693 phytoplankton, Global Biogeochemical Cycles, 13, 827-843, 1999.
694 Purina, I., Balode, M., Béchemin, C., Põder, T., Vérité, C., and Maestrini, S.: Influence of dissolved
695 organic matter from terrestrial origin on the changes of dinoflagellate species composition in the Gulf
696 of Riga, Baltic Sea, Hydrobiologia, 514, 127-137, 2004.
697 Rau, G., Riebesell, U., and Wolf-Gladrow, D.: A model of photosynthetic 13C fractionation by marine
698 phytoplankton based on diffusive molecular CO2 uptake, Marine Ecology Progress Series, 133, 275-
699 285, 1996.
700 Rau, G. H.: Variations in sedimentary organic δ13C as a proxy for past changes in ocean and
701 atmospheric CO2 concentrations. In: Carbon Cycling in the Glacial Ocean: Constraints on the Ocean's
702 Role in Global Change, Springer, 1994.
703 Salvadó, J. A., Tesi, T., Sundbom, M., Karlsson, E., Kruså, M., Semiletov, I. P., Panova, E., and
704 Gustafsson, Ö.: Contrasting composition of terrigenous organic matter in the dissolved, particulate
705 and sedimentary organic carbon pools on the outer East Siberian Arctic Shelf, Biogeosciences, 13,
706 6121-6138, 2016.

Sánchez-García, L., Alling, V., Pugach, S., Vonk, J., van Dongen, B., Humborg, C., Dudarev, O., Semiletov, I., and Gustafsson, Ö.: Inventories and behavior of particulate organic carbon in the Laptev and East Siberian seas, Global Biogeochemical Cycles, 25, 2011.

Semiletov, I., Dudarev, O., Luchin, V., Charkin, A., Shin, K. H., and Tanaka, N.: The East Siberian Sea as a transition zone between Pacific-derived waters and Arctic shelf waters, Geophysical Research Letters, 32, 2005.

Semiletov, I., Pipko, I., Gustafsson, O., Anderson, L. G., Sergienko, V., Pugach, S., Dudarev, O., Charkin, A., Gukov, A., Broder, L., Andersson, A., Spivak, E., and Shakhova, N.: Acidification of East Siberian Arctic Shelf waters through addition of freshwater and terrestrial carbon, Nature Geosci, 9, 361-365, 2016.

Semiletov, I. P., Shakhova, N. E., Pipko, I. I., Pugach, S. P., Charkin, A. N., Dudarev, O. V., Kosmach, D. A., and Nishino, S.: Space-time dynamics of carbon and environmental parameters related to carbon dioxide emissions in the Buor-Khaya Bay and adjacent part of the Laptev Sea, Biogeosciences, 10, 5977, 2013.

Sobek, A. and Gustafsson, Ö.: Latitudinal fractionation of polychlorinated biphenyls in surface seawater along a 62 N– 89 N transect from the southern Norwegian Sea to the North Pole area, Environmental science & technology, 38, 2746-2751, 2004.

Spreen, G., Kaleschke, L., and Heygster, G.: Sea ice remote sensing using AMSR-E 89-GHz channels, Journal of Geophysical Research: Oceans, 113, 2008.

Tesi, T., Muschitiello, F., Smittenberg, R. H., Jakobsson, M., Vonk, J. E., Hill, P., Andersson, A., Kirchner, N., Noormets, R., Dudarev, O., Semiletov, I., and Gustafsson, Ö.: Massive remobilization of permafrost carbon during post-glacial warming, Nature Communications, 7, 13653, 2016.

Tesi, T., Puig, P., Palanques, A., and Goñi, M.: Lateral advection of organic matter in cascading-dominated submarine canyons, Progress in Oceanography, 84, 185-203, 2010.

Tesi, T., Semiletov, I., Hugelius, G., Dudarev, O., Kuhry, P., and Gustafsson, Ö.: Composition and fate of terrigenous organic matter along the Arctic land–ocean continuum in East Siberia: Insights from biomarkers and carbon isotopes, Geochimica et Cosmochimica Acta, 133, 235-256, 2014.

Torres-Valdés, S., Tsubouchi, T., Bacon, S., Naveira-Garabato, A. C., Sanders, R., McLaughlin, F. A., Petrie, B., Kattner, G., Azetsu-Scott, K., and Whitledge, T. E.: Export of nutrients from the Arctic Ocean, Journal of Geophysical Research: Oceans, 118, 1625-1644, 2013.

Vonk, J., Sánchez-García, L., Van Dongen, B., Alling, V., Kosmach, D., Charkin, A., Semiletov, I. P., Dudarev, O. V., Shakhova, N., and Roos, P.: Activation of old carbon by erosion of coastal and subsea permafrost in Arctic Siberia, Nature, 489, 137-140, 2012.

Vonk, J. E., Semiletov, I. P., Dudarev, O. V., Eglinton, T. I., Andersson, A., Shakhova, N., Charkin, A., Heim, B., and Gustafsson, Ö.: Preferential burial of permafrost-derived organic carbon in Siberian-Arctic shelf waters, Journal of Geophysical Research: Oceans, 119, 8410-8421, 2014.

Wegner, C., Hölemann, J. A., Dmitrenko, I., Kirillov, S., Tuschling, K., Abramova, E., and Kassens, H.: Suspended particulate matter on the Laptev Sea shelf (Siberian Arctic) during ice-free conditions, Estuarine, Coastal and Shelf Science, 57, 55-64, 2003.

Wikner, J. and Andersson, A.: Increased freshwater discharge shifts the trophic balance in the coastal zone of the northern Baltic Sea, Global Change Biology, 18, 2509-2519, 2012.

Wolf-Gladrow, D. A., Riebesell, U., Burkhardt, S., and Bijma, J.: Direct effects of CO2 concentration on growth and isotopic composition of marine plankton, Tellus B, 51, 461-476, 1999.